Available online at www.sciencedirect.com
ScienceDirect
Catalysis Today 124 (2007) 110–117
CATALYSIS TODAY
www.elsevier.com/locate/cattod

Photocatalytic properties of screen-printed titania

D.S. Tsoukleris [a], A.I. Kontos [a], P. Aloupogiannis [b], P. Falaras [a,*]

[a] Institute of Physical Chemistry, NCSR "Demokritos", 15310 Aghia Paraskevi, Athens, Greece
[b] Institute of Materials Science, NCSR "Demokritos", 15310 Aghia Paraskevi, Athens, Greece

Available online 7 May 2007

Abstract

Nanocrystalline thin films of important surface roughness and complexity were prepared by screen-printing of commercial TiO_2 powder. The screen-printed titania films were tested in the photocatalytic decomposition reaction of methyl orange under UV light (350 nm). The photocatalytic activity strongly depends on the titania paste components and especially on the presence of a surface modifier (acetyl acetone) combined with a rheology controlling agent (ethyl cellulose). This results in improvement of the paste viscosity and optimization of the films morphology. Experiments under direct full sunlight illumination prove the importance of the screen-printed films for practical applications.

Keywords: Methyl orange; Photocatalysis; Screen-printing; TiO_2

1. Introduction

The necessity to find alternative solutions for environmental protection, led to the development of new solar technologies. Photocatalysis is an advanced oxidation process (AOP) that has received considerable attention in recent years as a viable degradation procedure for numerous pollutants [1,2]. Important research activity focuses on materials engineering for heterogeneous photocatalytic processes and applications [3–5]. It is well-established that titanium dioxide and related nanostructured materials in the presence of UV light can create very active species that are able to restore and preserve a clean environment, by decomposing harmful organics, killing bacteria and viruses and being easily self-cleaned [6].

Recent investigations insist on the photocatalyst immobilization in the form of a thin film, trying to improve the efficiency of photocatalytic processes [7]. This can be obtained via optimization of the material properties, especially rough surface morphology and high effective surface area that could increase the photocatalyst ability to capture the incident light [8]. Thus, new efficient photocatalysts based on nanostructured titania are developed and characterized. It is recognized that the film properties strongly depend on the deposition process. Usually, the deposition takes place using doctor blade, spin coating, or dip coating processes. In this direction and in order to enable industrial benefits resulting from perfect control of the preparation parameters that assure repeatability and reproducibility, rough, high surface area nanocrystalline and porous titania films, mainly in the anatase crystal phase, were recently prepared using the screen-printing method [9].

A number of water and air pollutants including phenols, aromatic hydrocarbons and azo-dyes, identified as hazardous substances by the US EPA [10], can be used as target compounds in photocatalysis. Azo-dyes are among the most harmful organic compounds [11–13]. These substances, (i.e. methyl orange, acid red, solvent yellow) are waste carcinogenetic products of high toxicity. Methyl orange particularly is used in the dyeing process causing serious environmental and health problems. For that reason, its removal is of the highest priority. Thus, in this work, the screen-printed titania films were tested in the photocatalytic decomposition reaction of methyl orange under both UV light (350 nm) and direct sunlight irradiation. A series of pastes based on commercial titania powder was used in order to examine the role of both solvent and binder-surface modifier on the photocatalytic efficiency of the resulting films.

2. Methods

2.1. Photocatalyst preparation

Screen-printing is a modern deposition technique, widely applied in industrial processes for electronic interconnections.

* Corresponding author. Tel.: +30 210 6503644; fax: +30 210 6511766.
E-mail address: papi@chem.demokritos.gr (P. Falaras).

0920-5861/$ – see front matter © 2007 Elsevier B.V. All rights reserved.
doi:10.1016/j.cattod.2007.03.029

The method is based on perforated screens with micrometer size ≪windows≫. Due to the industrial applicability of the screen-printing technique, synthetic methods aiming at preparing efficient pastes of titanium dioxide are of great interest. The composition and rheological characteristics of the precursor paste are crucial for the homogeneity, adherence and roughness of the final TiO_2 films [14]. TiO_2 thin films were prepared on microscopy glass slides and were used as the photocatalyst substrates. For the synthesis of new and efficient titania pastes based on organic solvent compatible for application in screen-printing processes, commercially available TiO_2 powder (Degussa P25) was thoroughly used, due to its nanoparticle characteristics and availability. Essential parameters, such as semiconductor–paste composition, addition of binder molecules and dispersion temperature are examined. Annealing conditions (temperature, time) is also a crucial factor, as the deposition of the manufactured films is followed by controlled thermal treatment to remove the organic load and assure effective interconnection of the semiconducting nanoparticles. Additionally screen-printer parameters that affect the morphology of the film, i.e. printing speed, screen dimension, perforated window diameter, screen-substrate distance and applied pressure, have also been examined.

In the three different pastes we developed, we examined the influence of both solvent and binder-surface modifier [9,15]. In the first paste (Paste 1), we used 2-ethyl-1-hexanol as solvent, 4-hydroxy-benzoic acid as acidification agent, ethyl cellulose as rheology agent, polyethylene glycol as binder. In the second case (Paste 2), acetyl acetone was added as surface modifier. The third one (Paste 3) was similar to Paste 1, with dibutylphtalate replacing 2-ethyl-1-hexanol in the role of the solvent. The pastes were screen-printed using EKRA Microtronic II instrumentation. The screen (Koenen GmbH, Germany) had the following characteristics: $w = 250$ μm, thread diameter $d = 120$ μm, open screen area $\alpha_0 = 46\%$, fabric thickness $D = 225$ μm, screen dimensions = 44 cm × 44 cm, screen material – polyester and squeegee material – plastic. The deposition of paste took place on microscope glass slides under the following conditions: Squeegee speed = 30 mm s^{-1}, distance between screen and substrate 1 mm, separation (leveling) speed 1 mm s^{-1}, applied squeegee pressure 7.5 atm and squeegee angle 80°. The glass substrates were ultrasonically cleaned in ethanol, prior to use. Thermal treatment of the printed films was a necessary step, in order to achieve removal of the organic load and facilitate sintering of titanium dioxide nanoparticles. Thus, TiO_2 thin films were heat treated at 150 °C for 30 min and annealed at 450 °C for exactly 90 min in an ambient atmosphere.

2.2. Characterization of TiO_2 films

The thickness of the screen-printed titania thin film photocatalysts was determined by profilometry (Model XP-2 of Ambios Technology) and found to be ∼20 μm. Surface morphology, roughness and fractality of the films were examined with a Digital Instrument Nanoscope III atomic force microscope (AFM), operating in the tapping mode (TM) [16,17]. This crystallinity was studied with a Siemens D-500 X-ray diffractometer, using Cu Kα radiation. Raman spectroscopy was employed to elucidate the vibrational modes of the semiconductor, using a triple Jobin–Yvon–Raman spectrometer equipped with a microscope and a CCD detector and a 514.5 nm argon laser. Detailed surface images were obtained by means of a scanning electron microscope (SEM) with numerical image acquisition (LEICA S440). Carbon deposition has been performed to avoid problems arising from surface charge effects. X-ray from the SEM microscope probe (at horizontal incidence beam) was used for non-destructive qualitative and quantitative chemical analysis of the modified films.

2.3. Photocatalysis experiments

The photocatalytic activity of the TiO_2 films was evaluated by degradation of methyl orange ([4-[[4-dimethylaminophenyl]-azo]benzenesulfonic acid sodium salt] with the molecular formula $[(CH_3)_2NC_6H_4N{=}NC_6H_4SO_3Na]$) or acid orange 52. Aqueous solutions of methyl orange (4 ml) were photolyzed in the presence of TiO_2 thin films, under magnetic stirring. The films initially deposited on microscopy glass substrates were adjusted accurately in surface area at 0.64 cm^2, by cutting the glass slides with a diamond knife. Photocatalysis experiments were carried out at round-bottomed photocatalytic cells. The cell glass permits radiation pass through when wavelength is over 320 nm. For cell illumination, an irradiation system equipped with four F15W/T8 black light blue light tubes (Sylvania GTE) was used (Scheme 1). The photon source has a maximum emission at 350 nm and emits 71.7 μW cm^{-2} at a distance of 25 cm. To check practical applicability, solar decomposition of the pollutant was also performed under solar irradiation, both direct and simulated. To confirm the accuracy of the measurements, the contaminant solution was also

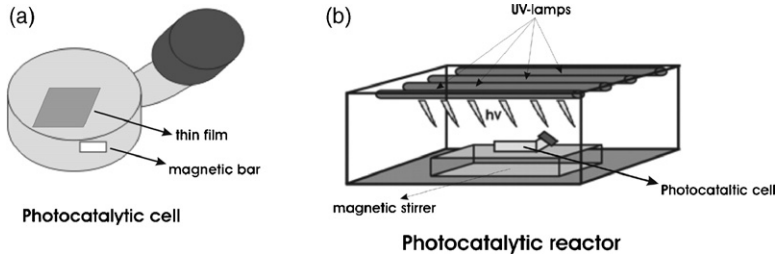

Scheme 1. Photocatalytic cell (a) and photoreactor/UV illumination system (b) for methyl orange (MO) photodegradation.

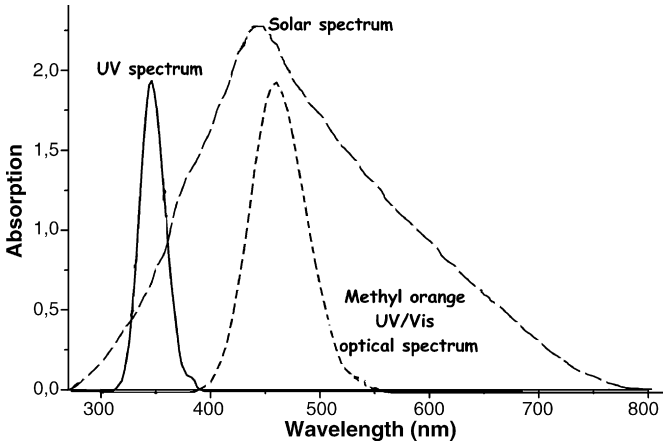

Fig. 1. Spectral distribution of UV and direct solar light in comparison with methyl orange UV/vis optical spectrum.

illuminated in the absence of photocatalyst to examine its stability. In every case, the experimental results verify that the azo-dye is not decomposed even after long-time irradiation. Methyl orange optical spectrum (Fig. 1) indicates that irradiation wavelengths around 350 nm cannot be absorbed by the dye molecule. The dye concentration was then measured using a Jasco (V-560) UV/vis spectrophotometer at a wavelength of 466.5 nm.

3. Results and discussion

3.1. Photo-catalyst characterization

The screen-printing pastes have been rheologically characterized, as the screen-printing process involves fluid motion during printing. The rheology analysis of the titania pastes showed a thixotropic (non-Newtonian) behavior and proved that their viscosity (η in mP s) follows the order: Paste 1(1.3×10^4) < Paste 2 (3.0×10^4) < Paste 3 (4.1×10^4) at a shear rate of 5 s^{-1} [18]. From these results we conclude that the pastes fit well the screen-printing requirements and their main characteristic is the absence of surfactant.

X-ray chemical analysis of the titania films after sintering at 450 °C, shown in Fig. 2, indicates a well-organized crystal structure of titania nanoparticles. The inset picture zooms at the A(1 0 1) anatase and R(1 1 0) rutile peaks in the region of 24–28°. The ratio of the two peak intensities was approximately the same (under the experimental error), for the new photocatalysts and Degussa P25 powder, indicating similar weight percentages of the anatase to rutile phases. The rutile content in the film is roughly 25%, while the anatase content is about 75%. This confirms that the initial crystalline composition remains in the modified catalysts. Furthermore, the grain size was determined from the width at half maximum (w_h) of the A(1 0 1) anatase peak according to Scherrer formula

$$D = \frac{0.9\lambda}{w_h \times \cos\theta} \quad (1)$$

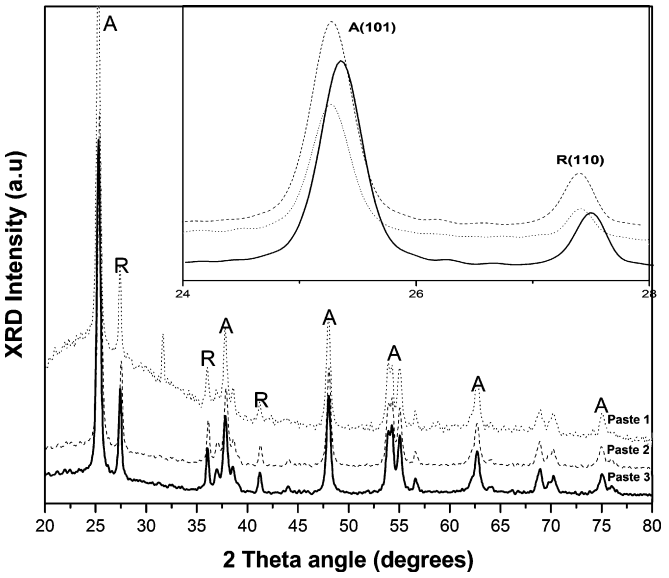

Fig. 2. The XRD patterns of titania photocatalysts resulting from three different screen-printing pastes.

Using Eq. (1), the particle size value D was estimated at about 24 nm for the three different catalysts.

Raman spectroscopy, a flexible, non-destructive technique for characterization of nanostructured semiconductors, is capable to elucidate the titania structural complexity as peaks from each crystalline phase are clearly separated in frequency, and therefore the anatase and rutile phases are easily distinguishable [16]. The Raman spectra (Fig. 3) prove that the materials are well-crystallized, without overlapped peaks and low number of imperfect sites. Vibration peaks at 142 ± 2 cm^{-1} (E_g, vs), 194 ± 3 cm^{-1} (E_g, w), 393 ± 2 cm^{-1} (B_{1g}, s), 512 ± 1 cm^{-1} (A_{1g}, s), 634 ± 2 cm^{-1} (E_g, s) are present in the Raman spectra of the TiO_2 nanocrystalline films, unambiguously attributed to the anatase modification. Although anatase nanoparticles are the predominant species, rutile phase is also observed as a broad peak at 446 cm^{-1} [19].

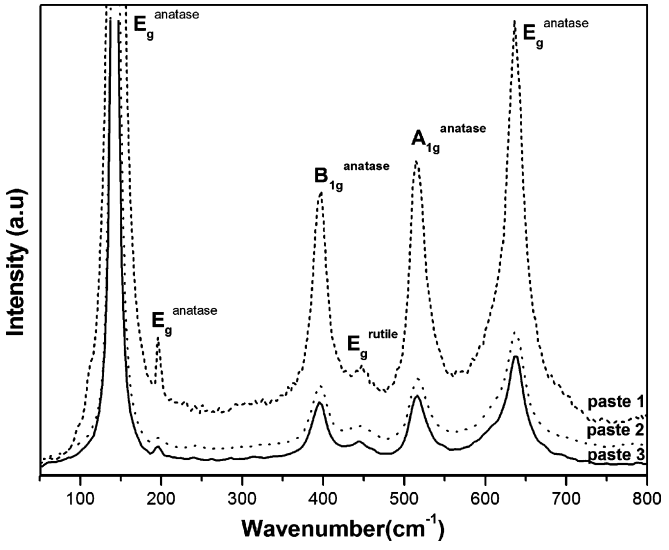

Fig. 3. Raman spectra for films resulting from Pastes 1, 2 and 3.

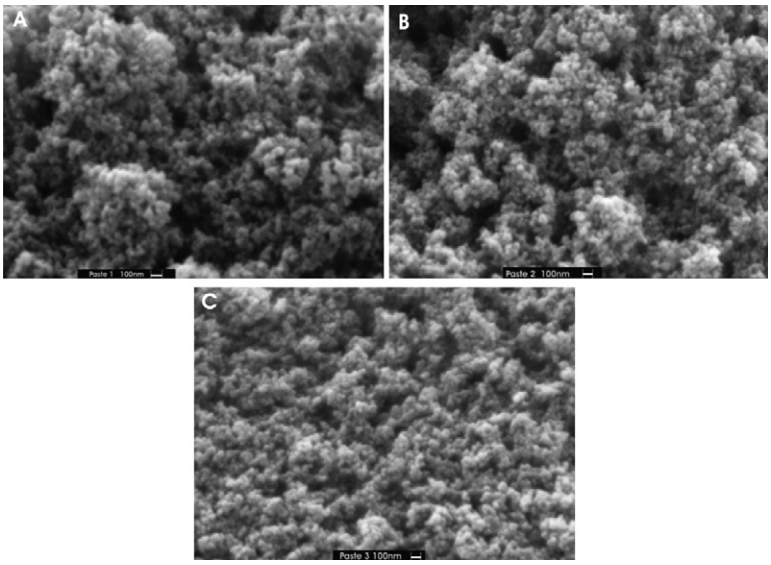

Fig. 4. Microscopic characterization (SEM) of the titania thin films resulting from the three screen-printing pastes.

The above results (XRD and Raman) can be understood on the basis of no alteration of the raw material charactreristics (TiO_2 Degussa P25) during the paste/film preparation processes.

Surface morphology, complexity and nanostructure are the most crucial factors for photochemically induced processes [16] especially efficient thin film photocalyst [17]. Analysis performed by means of scanning electron microscopy (SEM) (Fig. 4) revealed that the surface of the titania films possess a sponge like structure, with extended roughness and complex characteristics. The mean diameter of the nanocrystallites is controlled by the original semiconductor material, namely Degussa P25 and the analysis confirmed that modification with an organic carrier does not induce aggregation or additional growth of the TiO_2 nanoparticles. In general, the appearance of the films corresponds to a porous network with extended surface area, ideal for heterogeneous energy conversion processes, such as the photocatalytic procedure.

In order to better understand the titanium dioxide features and express this in terms of surface parameters, we have undertaken their characterization by atomic force microscopy (AFM). Fig. 5(A–C) presents surface plots for the modified film photocatalysts respectively. Interconnected grain particles with an average diameter of about 20 nm are fused together to form the three-dimensional network of high mountains and big valleys of the thin film semiconducting material. The investigation of morphological characteristics based on the comparison of height histograms and roughness analysis show that the Paste 3 produces uniform films with surface features of lower but more regular size.

The obtained titania films are opaque and besides an important roughness, they present complex surface characteristics confirmed by relatively high fractal dimension values. In fact, the corresponding fractal analysis performed in Fig. 6 following surface simulation using the equilateral triangle approach proved that the films have both self-similar and self-affine properties, corresponding to fractal dimension values as high as 2.22 (Table 1). It is worth mentioning that the titania films resulting from Paste 3 present the highest surface complexity and the higher frequency of surface features.

3.2. Photocatalytic activity

The photocatalysis experiments took place in an aqueous solution of methyl orange. The films, deposited on microscope glass slides were used for photocatalysis. The photocatalytic activity was evaluated as the percentage of pollutant disappearance. Methyl orange photodegradation kinetics under UV-illumination indicate a decrease of pollutant concentration in the presence (Fig. 7), that permit to directly compare the performance of our three different photocatalysts. Initial reaction conditions provide realistic comparison of the photodegradation rates, as it is clear that under the experimental conditions used, the photocatalytic curves follow first-order reaction kinetics, verified by the linear plots of Fig. 8.

Table 1
Apparent first-order rate constant (k_{app})*, photonic efficiency (Φ_λ) and fractal dimension (D_f) values for the screen-printed titania photocatalysts

TiO_2 photocatalyst	k_{app} (min^{-1})	Photonic efficiency, Φ_λ (%, at 1 s)	Fractal dimension, D_f
Film from Paste 1	0.023	23.3	2.190
Film from Paste 2	0.013	12.9	2.113
Film from Paste 3	0.026	26.4	2.222

*Reference test: for comparison, the corresponding value for an equivalent amount of non-supported Degussa P25 powder suspension, photolyzed under similar conditions, was found to be equal to 0.033 min^{-1}.

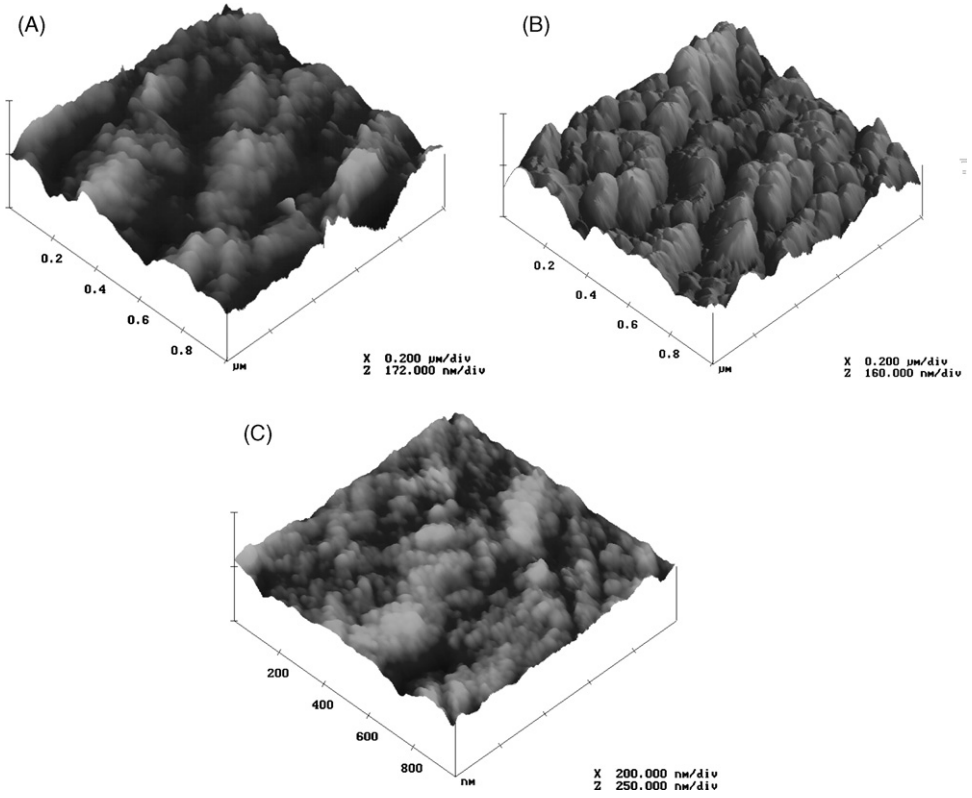

Fig. 5. Atomic force microscopy (AFM) images of the screen-printed photocatalysts: from Paste 1 (A); from Paste 2 (B); and from Paste 3 (C), respectively.

As a result, the photodegradation kinetics of methyl orange can be analyzed following the Langmuir–Hinshelwood model [20] generally observed when the pollutant is in the millimolar concentration range. In that case the reaction rate R is proportional to the surface coverage θ (Eq. (1))

$$R = -\frac{dC}{dt} = k_t\theta = \frac{k_r KC}{1 + KC} \tag{2}$$

where k_r is the reaction rate constant, K the adsorption coefficient of the reactant and C is the reactant concentration. When C is very small, the product KC is negligible with respect to unity so that Eq. (2) describes a first-order kinetics. Integration of Eq. (2) between the initial conditions (t = 0, Co) and (t, C) gives Eq. (3)

$$-\ln\left(\frac{C}{C_0}\right) = k_{app}t \tag{3}$$

where C_o is the initial concentration and $k_{app}(=k_rK)$ is the apparent first-order reaction constant.

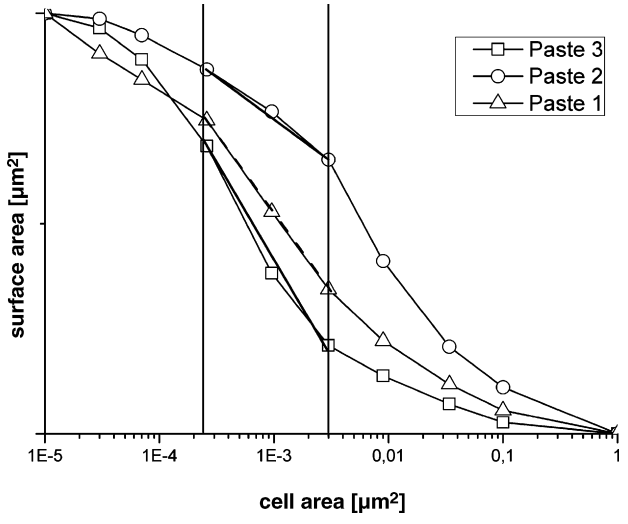

Fig. 6. Fractal analysis on the screen-printed thin film photocatalysts.

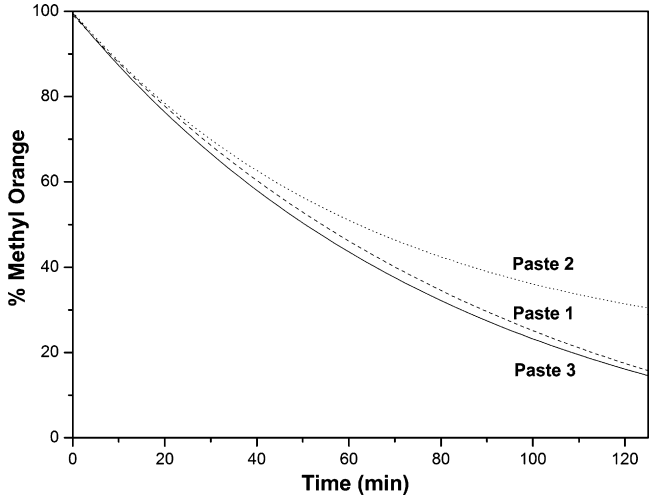

Fig. 7. Photodecomposition kinetics of methyl orange using TiO_2 thin film catalysts (Paste 1: with 2-ethyl-1-hexanol; Paste 2: with 2-ethyl-1-hexanol and acetyl acetone, Paste 3: only with dibutylphthalate).

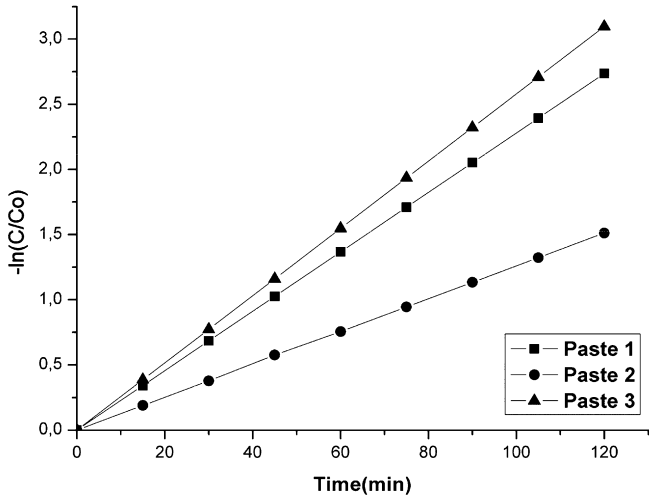

Fig. 8. Linear plots of photodegradation kinetiks of methyl orange using screen-printed titania photocatalysts.

The apparent first-order rate constants, resulting from the linear plots in Fig. 8 by applying Eq. (3), are summarized in Table 1.

Usually changes in k_{app} are attributed, via Eq. (3), to corresponding variations in the K values, i.e. to the different absorption of the reactant in the surface of the semiconductor nanoparticles or equivalently to different surface coverage θ. In our case, particularly, differences in k_{app} are attributed to the photocatalyst characteristic properties, especially structural morphology and real surface area, as the average particle diameter remains the same. In addition, it is clear from Table 1 that the higher the surface complexity, the higher the apparent first-order rate constant and therefore the higher the photocatalytic efficiency. This can be understood in terms of the photocatalyst surface area (S) exposed to the light beam. It is well-established that a complex surface with high fractal dimension (D_f) value results to a real surface area (S depends exponentially on D_f) significantly higher than that corresponding to a non-fractal one [21].

In heterogeneous photocatalysis however, the photonic efficiency, Φ_λ, can be used to describe the rate of decomposed molecules (M) relative to the total rate of photons incident on the reactor (L)

$$\Phi_\lambda = \frac{M}{L} \tag{4}$$

The number of pollutant molecules (for a volume of 4 ml) decomposed within time t is given by

$$M_t = \left(\frac{4}{1000}\right) C_0 N (1 - e^{-kt}) \tag{5}$$

Where, C_0 is the pollutant initial concentration (2.056 mol/l), N the Avogadro's number (6.023×10^{23}) and k is the apparent first-order reaction constant (s^{-1}).

The number of incident photons within time t is given by

$$L_t = \frac{P\lambda t}{hc} \tag{6}$$

where P is the light power (45.88×10^{-6} W), λ the wavelength ($350 \times 10^{-9} \times$ m), h the Plank's constant (6.63×10^{-34} J s) and c is the velocity of light in the vacuum (3×10^8 m s^{-1}).

Eqs. (4)–(6) can help us to obtain a first approximation on the quantum efficiency of the decomposition process. In fact, considering a decomposition time as short as 1 s, this efficiency corresponds to the so-called "initial photonic efficiency" value. It also constitutes a lower limit of the actual quantum yield, based on the assumption that all the incident photons are absorbed by the photocatalyst (the solid photocatalyst surface in our case). By taking into account the apparent first-order decomposition rate constants, Eq. (4) gives the initial efficiency values, reported in Table 1. It is clear that for the best titania thin film catalyst (resulting from Paste 3), the quantum efficiency is as high as 26%. However, it must be taken into account that the above calculated Φ_λ values are not standardized, as the number of absorbed photons is experimentally difficult to access. In order to compare our data, a reference test was performed with an equivalent amount of non-supported Degussa P25. For that the film weight (from Paste 3) was measured and the concentration of a Degussa P25 slurry was adjusted to meet the exact quantity of the immobilized film. The pollutant was mixed with the powder dispersion and was photolyzed under the same conditions as in the case of the thin films. The results, incorporated into Table 1, show that the apparent first-order rate constant (k_{app}) equals 0.033 m^{-1}, slightly higher than that of the corresponding values of the supported samples. Such a difference can be understood, taking into account that photocatalysis is a surface phenomenon, requiring direct contact between the pollutant and the semiconductor. However, in the particular case of the immobilized systems the relative efficiency (about 79%) is considered to be high enough, as only the external surface (and not the integrity) of the photocatalyst is available.

Water decontamination by means of solar energy is very attractive, low cost alternative of particular technological interest and high importance, especially because of the magnitude of the environmental problem and its urgent character. In order to check the potentiality of the titania screen-printed films for practical applications, solar detoxification experiments were performed [22]. Thus, the photodecomposition of the pollutant was investigated under direct sunlight irradiation (at a mean irradiance of 778 W m^{-2}) and the results are reported in Fig. 9. Even with natural solar light, the catalysts confirm their photodegradation ability. Their relative efficiency order is also maintained with the film resulting from Paste 3 to be the best photocatalyst.

It must be pointed out that due to the strong adherence of the materials onto the glass substrate and their photochemical stability, the photocatalysts retain their activity and no mass loss was observed after prolonged use. In addition, under UV illumination, the corresponding parameters (reaction constants, k and photonic efficiencies, Φ_λ) for the titania screen-printed films remains unmodified after 10 consecutive experiments of new added pollutant (MO), Fig. 10. This is in agreement with AFM investigations performed on the samples surface after 10 photocatalysis runs. The analysis of the obtained pictures

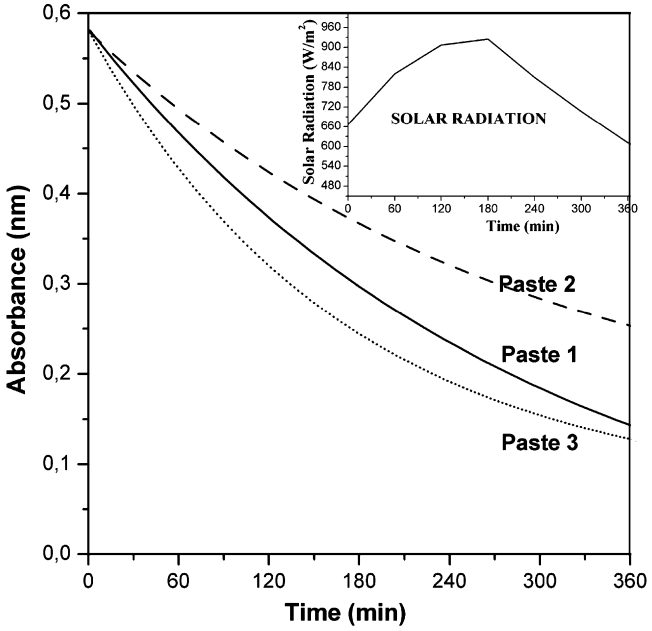

Fig. 9. Photodegradation of methyl orange under direct sunlight irradiation.

confirmed that the film morphology and surface characteristics are nor affected and main parameters, such as surface roughness (R_{ms}) and complexity (fractal dimension, D_f) have practically the same values as those taken on the virgin samples. In addition, under these conditions the materials structure remains intact as both XRD and Raman investigations did not confirm any variation on the anatase/rutile ratio.

3.3. Photocatalysis mechanism

The basic photochemical process requires photons that are directly absorbed by the catalyst and/or the reactants, causing a chemical reaction. As we have to deal with a colored pollutant presenting strong absorption in the visible, the particular point here is to clarify if the photodegradation reaction involves direct or/and sensitized pathways. To answer this question, the illumination system must be taken into account.

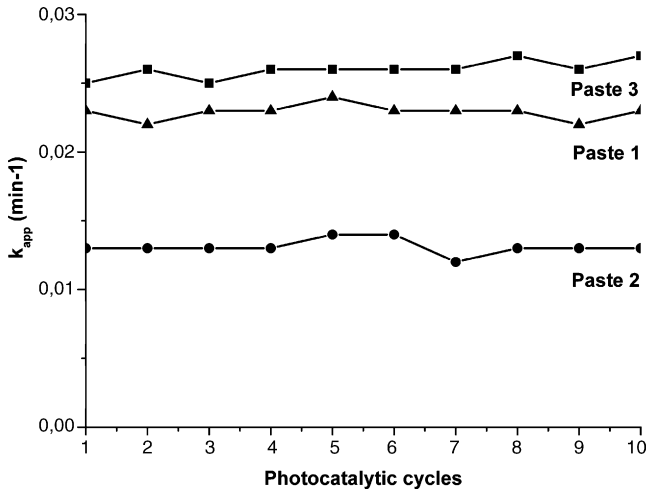

Fig. 10. Photodegradation of methyl orange under UV (350 nm) illumination. Variation of the reaction constants (k) for the titania screen-printed films during 10 consecutive experiments of new added pollutant.

UV light illumination: methyl orange optical spectrum (Fig. 1) indicates that irradiation wavelengths around 350 nm cannot be absorbed by the dye molecule, excluding thus the sensitized photocatalysis route. It is now well-established that the photocatalysis mechanism involves the participation of surface hydroxyls (OH^-). In the case of UV illumination, absorption of photons of energy greater than the band gap energy (E_g = 3.0 for rutile or 3.2 eV for anatase) creates pairs of electrons (e^-) and holes (h^+). In the valence band, the photogenerated holes migrate to the interface and react with OH^- adsorbed onto the TiO_2 to create hydroxyl radicals ($^\bullet OH$). The $^\bullet OH$ radicals present extremely strong oxidizing properties and are able to decompose the MO pollutant. It is then expected that materials rich in surface hydroxyls (and therefore in resulting $^\bullet OH$ radicals) present, respectively, high photocatalytic activity.

Solar light illumination: in this case however, one must have in mind that the heterogeneous photocatalysis is a more complex process and might also include the mechanism of sensitized photocatalysis [23,24]. This is different from the UV irradiation mechanism, very typical for coloured pollutants photodegradation. The mechanism involves absorption of visible photons by the pollutant molecule and creation of a dye (pollutant) excited state and the resulting cation radical by electron injection into then semiconductor conduction band. The later is a very instable species that easily reacts with molecular oxygen, dioxygen or hydroxyl radicals leading to degraded intermediates and/or mineralized products. However, the use of solar simulated light (AM 1.5) from a 300 W Xe lamp using a 400 nm cut-off filter did not lead to any discoloration of the MO pollutant, thus confirming that the sensitized photocatalysis route is forbidden, under the present experimental conditions.

4. Conclusions

The three screen-printed catalysts have different characteristic properties, strongly dependent on the paste components. This results in differences in the titania total surface area exposed to the light beam and to that available for pollutant adsorption. The above explanation is consistent with the highest photocatalytic activity observed for the material resulting from Paste 3, which presents the highest complexity and real surface area. Microscopy analysis (SEM and AFM) indicates that the films with acetyl acetone had better morphology without cracks. This fact underlines the ability of acetyl acetone to make qualitative titania thin films. Therefore, the corresponding film is able to absorb the incident light more efficiently and show enhanced photocatalytic performance.

As it usually happens with the whole family of the colored pollutants and especially the azo-dyes, the role of the light source is crucial in order to describe the photocatalytic process. In the particular case of methyl orange (MO), the analysis of the obtained results is consistent with the direct photocatalysis mechanism, excluding the existence of a parallel sensitization pathway. In addition, full sunlight irradiation experiments

confirmed the viability of the screen-printing deposition technique for practical applications, especially in terms of solar detoxification of polluted water.

Acknowledgements

Great acknowledgements are expressed for financial support from GSRT/Ministry of Development-Greece (03ED963 PENED project). Thanks must also be addressed to Degussa AG Frankfurt, Germany and Delis AE Athens, Greece, for generously providing the TiO_2 Degussa P25 powder. We appreciate the valuable assistance from Dr. V. Psycharis for the XRD analysis and M.C. Bernard for the Raman spectra and the SEM images.

References

[1] H. Al-Ekabi, N. Serpone, J. Phys. Chem. 92 (1988) 5726.
[2] O.M. Alfano, D. Bahnemann, A.E. Cassano, R. Dillert, R. Goslich, Catal. Today 58 (2000) 199.
[3] A. Fujishima, K. Hashimoto, T. Watanabe, TiO_2 Photocatalysis, Fundamentals and Applications, BKC, Inc., Tokyo, 1999.
[4] A. Fujishima, T.N. Rao, D.A. Tryk, J. Photochem. Photobiol. C: Photochem. Rev. 1 (2000) 1.
[5] I. Sopyan, M. Watanabe, S. Murasawa, K. Hashimoto, A. Fujishima, J. Photochem. Photobiol. A 98 (1996) 79.
[6] H.M. Coleman, C.P. Marquis, J.A. Scott, S.S. Chin, R. Amal, Chem. Eng. J. 113 (2005) 55.
[7] G. Balasubramanian, D.D. Dionysiou, M.T. Suidan, I. Baudin, J.-M. Laîné, Appl. Catal. B: Environ. 47 (2004) 73.
[8] V. Subramanian, E.E. Wolf, P.V. Kamat, J. Am. Chem. Soc. 126 (2004) 4943.
[9] D.S. Tsoukleris, I.M. Arabatzis, E. Chatzivasiloglou, A.I. Kontos, V. Belessi, M.C. Bernard, P. Falaras, J. Solar Energy 9 (2005) 422.
[10] J.B. Galvez, S.M. Rodríguez, Solar Detoxification, United Nations Educational, 2003,, p. 2.
[11] A. Patsoura, D.I. Kondarides, X.E. Verykios, Appl. Catal. B: Environ. 64 (2006) 171.
[12] T. Velegraki, I. Poulios, M. Charalabaki, N. Kalogerakis, P. Samaras, D. Mantzavinos, Appl. Catal. B: Environ. 62 (2006) 159.
[13] P. Bouras, E. Stathatos, P. Lianos, C. Tsakiroglou, Appl. Catal. B: Environ. 51 (2004) 275.
[14] S.B. Hoff, Screen Printing: A Contemporary Approach, Delmar Publishers, NY, 1997, p. 12.
[15] Y.J. Chen, D.D. Dionysiou, J. Mol. Catal. A-Chem. 244 (2006) 73.
[16] P. Falaras, Sol. Energy Mater. Sol. Cells 53 (1998) 163.
[17] P. Falaras, A.P. Xagas, J. Mater. Sci. 37 (2002) 3855.
[18] T.C. Patton, Paint flow and Pigment Dispersion, John Wiley and Sons, New York, 1979, p. 5.
[19] T. Stergiopoulos, M.C. Bernard, A.H. Le-Goff, P. Falaras, Coord. Chem. Rev. 248 (2004) 1407.
[20] V. Augugliaro, S. Coluccia, E. Garcia-Lopez, V. Loddo, G. Marci, G. Martra, L. Palmisano, M. Schiavello, Top. Catal. 35 (2005) 237.
[21] A. Provata, P. Falaras, A. Xagas, Chem. Phys. Lett. 297 (1998) 484.
[22] M. Kositzi, A. Antoniadis, I. Poulios, I. Kiridis, S. Malato, Solar Energy 77 (2004) 591.
[23] M. Stylidi, D.I. Kondarides, X.E. Verykios, Appl. Catal. B: Environ. 47 (2004) 189.
[24] S. Dieckman, K.A. Gray, Water Res. 30 (1996) 1169.